SUPPORTING INFORMATION

Selective Characterization of Microsecond Motions in Proteins by NMR Relaxation

D. Flemming Hansen[a], Haniqiao Feng[b], Zheng Zhou[b], Yawen Bai[b], Lewis E. Kay[a]

(a) Departments of Molecular Genetics, Biochemisty and Chemistry, The University of Toronto, Toronto, Ontario, Canada, M5S 1A8

(b) Laboratory of Biochemistry and Molecular Biology, Center for Cancer Research, NCI, NIH, Bethesda, Maryland 20892, USA.

Chemical exchange in protein L is fast on the NMR chemical shift time-scale.

Amide proton $R_{1\rho}$ decay rates in protein L were acquired using a pulse sequence published previously[1]. The following spin-lock values (offset, field strength) were used: (9.57ppm, 1.6 kHz); (9.57ppm, 1.9 kHz); (9.57ppm, 2.4 kHz); (9.57ppm, 3.0kHz); (9.57ppm, 3.8 kHz); (9.57ppm, 4.8 kHz); (9.57ppm, 6.3kHz); (9.57ppm, 7.9 kHz); (9.57ppm, 10.2 kHz); (9.57ppm, 12.8 kHz); (22.1ppm, 3.0 kHz). For each offset, field strength $R_{1\rho}$ rates were derived by fitting a single exponential function, $A \exp(-R_{1\rho}\tau)$, to the decays of the signal intensity sampled at eight relaxation time-points, τ, of (0ms, 4ms, 8ms, 12ms, 18ms, 24ms, 32ms). Subsequently, the $R_{1\rho}$ rates were analyzed to derive the

rate constant of the chemical exchange event, k_{ex}, as described in the legend to Fig S1. For all amide protons of protein L, the exchange rate is faster than 4000 s^{-1}.

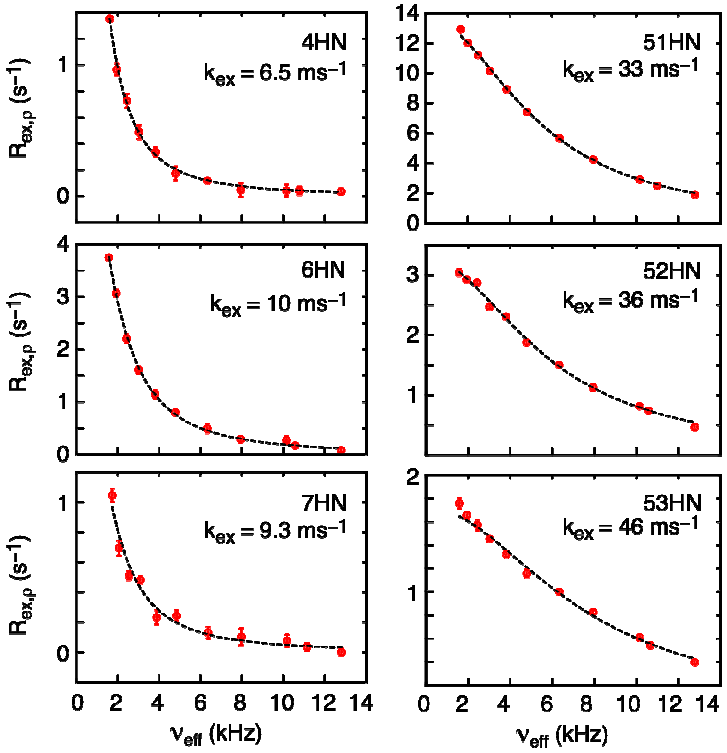

Figure S1. ^{1}H $R_{ex,\rho}$ values for protein L measured at a static magnetic field strength of 18.79 T and at a temperature of 278 K. The effective field, ν_{eff} was calculated as $\sqrt{\nu_1^2 + \nu^2}$, where ν_1 is the field strength of the spin-lock field (Hz) and ν is the offset from the rf-carrier (Hz). The exchange contributions to the proton relaxation, $R_{ex,\rho}$, are calculated as $(R_{1\rho} - R_1 \cos^2\theta_H)/\sin^2\theta - R_{2,0}$, where R_1 is the longitudinal relaxation rate, $R_{2,0}$ is the transverse relaxation rate in the absence of chemical exchange and $\tan\theta_H = \nu_1/\nu$. The dotted lines are least-squares fits of Eq. [8] (see text) to experimental $R_{ex,\rho}$ rates, where k_{ex}, $\Phi = p_A p_B \Delta\omega^2$, $R_{2,0}$, and R_1 are adjustable parameters. The obtained k_{ex} values are shown in each panel.

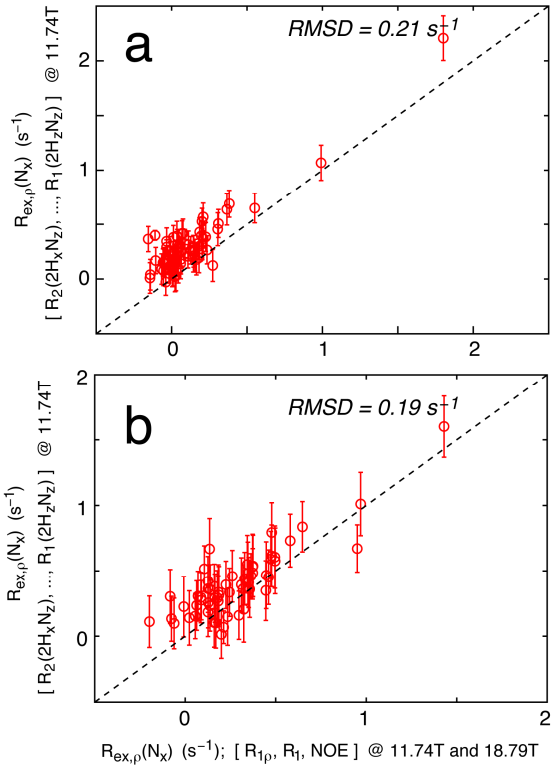

Figure S2. Exchange contributions $R_{ex,\rho}(N_x)$ obtained from measurement of residue-specific $R_2(2H_xN_z)$, $R_2(2H_zN_x)$, $R_2(2H_xN_x)$ and $R_1(2H_zN_z)$ relaxation rates at a magnetic field strength of 11.7 T (y-axis) agree with the corresponding values isolated from ^{15}N R_1, ^{15}N $R_{1\rho}$ and ^{1}H-^{15}N NOE measurements at two static magnetic fields (11.7 T and 18.8 T) for U-^{2}H,^{15}N labeled human ubiquitin at 298 K (a) and U-^{2}H,^{15}N labeled protein L at 278 K (b). A ^{15}N spin-lock field strength of 2 kHz was used for all experiments. The dotted lines correspond to y=x and the RMSD is calculated as $\sqrt{\Sigma(x_i - y_i)^2 / N}$.

Validation of the approximation $R_{ex}(H_x)+R_{ex}(N_x) \approx R_{ex}(H_xN_x)$.

The relation $R_{ex}(H_x)+R_{ex}(N_x) \approx R_{ex}(H_xN_x)$ has been used in the derivation of Eq. [7] that is the central equation of the paper and here we show that this approximation is indeed

valid for the complete range of possible chemical exchange scenarios. As shown below the approximation is exact in the limit of free-precession and fast chemical exchange, while $|\{R_{ex,\rho}(H_xN_x)-R_{ex,\rho}(H_x)-R_{ex,\rho}(N_x)\}/R_{ex,\rho}(N_x)| < 2\%$ in other cases, illustrated by numerical simulations. For free-precession and in the limit of fast-exchange the individual exchange contributions are:

$$R_{ex}(H_x)=\frac{p_B(1-p_B)\Delta\omega_H^2}{k_{ex}} \quad [S1]$$

$$R_{ex}(N_x)=\frac{p_B(1-p_B)\Delta\omega_N^2}{k_{ex}} \quad [S2]$$

$$R_{ex}(H_xN_x - H_yN_y)=\frac{p_B(1-p_B)(\Delta\omega_H+\Delta\omega_N)^2}{k_{ex}} \quad [S3]$$

$$R_{ex}(H_xN_x + H_yN_y)=\frac{p_B(1-p_B)(\Delta\omega_H-\Delta\omega_N)^2}{k_{ex}}. \quad [S4]$$

The relaxation rate of $R_{1\rho^2}(2H_xN_x)$ is monitored while simultaneous proton and nitrogen spin-locks of very different strengths are applied that effectively interconvert double- ($2H_xN_x$-$2H_yN_y$) and zero- ($2H_xN_x$+$2H_yN_y$) quantum coherences. Thus,

$$\begin{aligned} R_{ex}(2H_xN_x) &= (R_{ex}(H_xN_x + H_yN_y)+R_{ex}(H_xN_x - H_yN_y))/2 \\ &= \frac{p_B(1-p_B)}{2k_{ex}}\left\{\Delta\omega_H^2+\Delta\omega_N^2-2\Delta\omega_H\Delta\omega_H+\Delta\omega_H^2+\Delta\omega_N^2+2\Delta\omega_H\Delta\omega_H\right\} \\ &= \frac{p_B(1-p_B)}{k_{ex}}\left\{\Delta\omega_H^2+\Delta\omega_N^2\right\} \\ &= R_{ex}(H_x)+R_{ex}(N_x) \end{aligned} \quad [S5]$$

The validity of this approximation outside the fast-exchange regime was investigated with numerical simulations where decay curves of H_x, N_x, and $2H_xN_x$ were generated using the Liouvillian operator of Allard et. al[2]. A 13 kHz proton spin-lock field (x-direction) was applied for the H_x decay, a 2 kHz nitrogen spin-lock field (x-direction) was

employed for the N_x decay, and simultaneous proton (13 kHz) and nitrogen (2 kHz) spin-lock fields were applied for simulation of the decay of $2H_xN_x$. A two-site chemical exchange model, A⇌B, was assumed with an excited state population of 5% and difference in proton chemical shifts of $\Delta\varpi_H$=2.3ppm (the maximum amide proton chemical shift difference observed previously in a protein folding study)[3]. In Fig. S3 the difference $R_{ex,\rho}(H_xN_x) - R_{ex,\rho}(H_x) - R_{ex,\rho}(N_x)$ is shown for a range of values of k_{ex} and $\Delta\varpi_N$. The derived differences are very small, clearly establishing that the approximation $R_{ex}(H_x)+R_{ex}(N_x) \approx R_{ex}(H_xN_x)$ is valid, a necessary condition for the accuracy of Eq. [7].

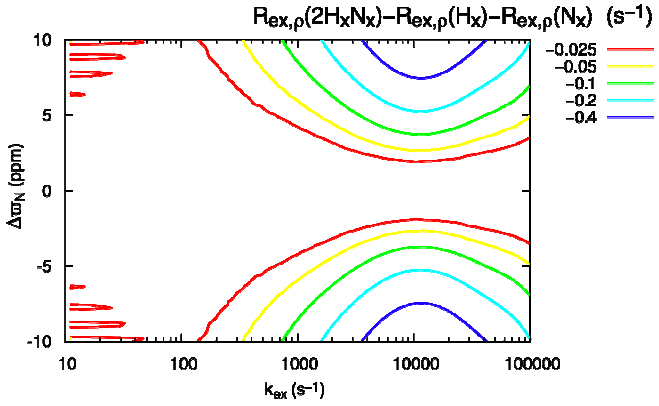

Figure S3. The difference, $R_{ex,\rho}(H_xN_x) - R_{ex,\rho}(H_x) - R_{ex,\rho}(N_x)$, simulated for a range of $\Delta\varpi_N$ and k_{ex} values. A proton (nitrogen) spin-lock field strength of 13 kHz (2kHz) was employed together with $\Delta\varpi_H$ = 2.3 ppm and p_B = 5%. Nitrogen $R_{ex,\rho}(N_x)$ values larger than $50s^{-1}$ are observed in the region where $R_{ex,\rho}(H_xN_x) - R_{ex,\rho}(H_x) - R_{ex,\rho}(N_x) < -0.4\ s^{-1}$, thus resulting in small fractional errors of the derived exchange contributions; indeed for all of the simulations $|\{R_{ex,\rho}(H_xN_x)-R_{ex,\rho}(H_x)-R_{ex,\rho}(N_x)\}/R_{ex,\rho}(N_x)| < 2\%$.

Derivation of Equation 7.

Consider the linear combination on the right hand side of Eq. [7] (first 2 lines). Substituting expressions from Eqs. [1-4] and collecting like-terms we obtain the following multipliers for each of the elements listed below.

<u>$J(0)$:</u>

$$\frac{1}{2}\left\{0\left(-1+\frac{4c_N^2}{3d_{HN}^2}\right)+\left(\frac{4d_{HN}^2}{8}+\frac{4c_N^2}{6}\right)\left(1-\frac{4c_N^2}{3d_{HN}^2}\right)+\left(\frac{4d_{HN}^2}{8}\right)\left(-1-\frac{4c_N^2}{3d_{HN}^2}\right)+\left(\frac{4c_N^2}{6}\right)\left(1+\frac{4c_N^2}{3d_{HN}^2}\right)\right\}=$$
$$\frac{1}{2}\left\{\frac{d_{HN}^2}{2}-\frac{2c_N^2}{3}+\frac{2c_N^2}{3}-\frac{8c_N^4}{9d_{HN}^2}-\frac{d_{HN}^2}{2}-\frac{2c_N^2}{3}+\frac{2c_N^2}{3}+\frac{8c_N^4}{9d_{HN}^2}\right\}=0$$

<u>$J(\omega_N)$:</u>

$$\frac{1}{2}\left\{\left(\frac{6d_{HN}^2}{8}+c_N^2\right)\left(-1+\frac{4c_N^2}{3d_{HN}^2}\right)+\left(\frac{3d_{HN}^2}{8}+\frac{3c_N^2}{6}\right)\left(1-\frac{4c_N^2}{3d_{HN}^2}\right)+c_N^2\left(-1-\frac{4c_N^2}{3d_{HN}^2}\right)+\left(\frac{3d_{HN}^2}{8}+\frac{3c_N^2}{6}\right)\left(1+\frac{4c_N^2}{3d_{HN}^2}\right)\right\}=$$
$$\frac{1}{2}\left\{-\frac{6d_{HN}^2}{8}+c_N^2-c_N^2+\frac{4c_N^4}{3d_{HN}^2}+\frac{3d_{HN}^2}{8}-\frac{c_N^2}{2}+\frac{c_N^2}{2}-\frac{2c_N^4}{3d_{HN}^2}-c_N^2-\frac{4c_N^4}{3d_{HN}^2}+\frac{3d_{HN}^2}{8}+\frac{c_N^2}{2}+\frac{c_N^2}{2}+\frac{2c_N^4}{3d_{HN}^2}\right\}=$$
$$0\times d_{HN}^2+0\times c_N^2+\frac{0\times c_N^4}{d_{HN}^2}=0$$

<u>$J(\omega_H+\omega_N)$:</u>

$$\frac{1}{2}\left\{0\left(-1+\frac{4c_N^2}{3d_{HN}^2}\right)+\frac{6d_{HN}^2}{8}\left(1-\frac{4c_N^2}{3d_{HN}^2}\right)+\frac{6d_{HN}^2}{8}\left(-1-\frac{4c_N^2}{3d_{HN}^2}\right)+\frac{6d_{HN}^2}{8}\left(1+\frac{4c_N^2}{3d_{HN}^2}\right)\right\}=$$
$$\frac{1}{2}\left\{\frac{3d_{HN}^2}{4}-c_N^2\right\}=\frac{3d_{HN}^2}{8}-\frac{c_N^2}{2}$$

<u>$J(\omega_H)$:</u>

$$\frac{1}{2}\left\{\frac{6d_{HN}^2}{8}\left(-1+\frac{4c_N^2}{3d_{HN}^2}\right)+0\left(1-\frac{4c_N^2}{3d_{HN}^2}\right)+\frac{3d_{HN}^2}{8}\left(-1-\frac{4c_N^2}{3d_{HN}^2}\right)+\frac{3d_{HN}^2}{8}\left(1+\frac{4c_N^2}{3d_{HN}^2}\right)\right\}=$$
$$-\frac{3d_{HN}^2}{8}+\frac{c_N^2}{2}$$

<u>$J(\omega_H-\omega_N)$:</u>

$$\frac{1}{2}\left\{0\left(-1+\frac{4c_N^2}{3d_{HN}^2}\right)+\frac{d_{HN}^2}{8}\left(1-\frac{4c_N^2}{3d_{HN}^2}\right)+\frac{d_{HN}^2}{8}\left(-1-\frac{4c_N^2}{3d_{HN}^2}\right)+\frac{d_{HN}^2}{8}\left(1+\frac{4c_N^2}{3d_{HN}^2}\right)\right\}=$$
$$\frac{d_{HN}^2}{16}-\frac{c_N^2}{12}$$

$\underline{\lambda_N}$:

$$\frac{1}{2}\left\{1\left(-1+\frac{4c_N^2}{3d_{HN}^2}\right)+0\left(1-\frac{4c_N^2}{3d_{HN}^2}\right)+1\left(-1-\frac{4c_N^2}{3d_{HN}^2}\right)+0\left(1+\frac{4c_N^2}{3d_{HN}^2}\right)\right\}=-1$$

$\underline{\vartheta_N}$:

$$\frac{1}{2}\left\{0\left(-1+\frac{4c_N^2}{3d_{HN}^2}\right)+1\left(1-\frac{4c_N^2}{3d_{HN}^2}\right)+0\left(-1-\frac{4c_N^2}{3d_{HN}^2}\right)+1\left(1+\frac{4c_N^2}{3d_{HN}^2}\right)\right\}=1$$

$\underline{\lambda_H}$:

$$\frac{1}{2}\left\{1\left(-1+\frac{4c_N^2}{3d_{HN}^2}\right)+1\left(1-\frac{4c_N^2}{3d_{HN}^2}\right)+0\left(-1-\frac{4c_N^2}{3d_{HN}^2}\right)+0\left(1+\frac{4c_N^2}{3d_{HN}^2}\right)\right\}=0$$

$\underline{\vartheta_H}$:

$$\frac{1}{2}\left\{0\left(-1+\frac{4c_N^2}{3d_{HN}^2}\right)+0\left(1-\frac{4c_N^2}{3d_{HN}^2}\right)+1\left(-1-\frac{4c_N^2}{3d_{HN}^2}\right)+1\left(1+\frac{4c_N^2}{3d_{HN}^2}\right)\right\}=0$$

$\underline{R_{ex}}$:

$$\frac{1}{2}\left\{0\left(-1+\frac{4c_N^2}{3d_{HN}^2}\right)+R_{ex,\rho}(N_x)\left(1-\frac{4c_N^2}{3d_{HN}^2}\right)+R_{ex,\rho}(H_x)\left(-1-\frac{4c_N^2}{3d_{HN}^2}\right)+\underbrace{R_{ex,\rho}(2H_xN_x)}_{R_{ex,\rho}(N_x)+R_{ex,\rho}(H_x)}\left(1+\frac{4c_N^2}{3d_{HN}^2}\right)\right\}$$

$$=R_{ex,\rho}(N_x)$$

Thus,

$$\frac{1}{2}\left\{R_1(2H_zN_z)\left(-1+\frac{4c_N^2}{3d_{HN}^2}\right)+R_2(2H_zN_x)\left(1-\frac{4c_N^2}{3d_{HN}^2}\right)+R_2(2H_xN_z)\left(-1-\frac{4c_N^2}{3d_{HN}^2}\right)+R_2(2H_xN_x)\left(1+\frac{4c_N^2}{3d_{HN}^2}\right)\right\}=$$

$$\left(\frac{d_{HN}^2}{16}-\frac{c_N^2}{12}\right)\left(J(\omega_H-\omega_N)+6J(\omega_H+\omega_N)\right)+\left(-\frac{3d_{HN}^2}{8}+\frac{c_N^2}{2}\right)J(\omega_H)-\lambda_N+\vartheta_N+R_{ex,\rho}(N_x)\approx$$

$$(0.106d_{HN}^2-0.1409c_N^2)J(0.87\omega_H)-\lambda_N+\vartheta_N+R_{ex,\rho}(N_x)\approx$$

$$0.035(3d_{HN}^2-4c_N^2)J(0.87\omega_H)-\lambda_N+\vartheta_N+R_{ex,\rho}(N_x)$$ Q.E.D.

From here, Eq. [7] follows by simple rearrangement of terms.

Concentration dependence of $R_{ex,\rho}$.

Microsecond chemical exchange contributions, $R_{ex,\rho}(N_x)$, for both protein L and human ubiquitin were measured at two different protein concentrations in order to establish whether aggregation is contributing to the observed exchange rates. Figures S4 and S5 establish that $R_{ex,\rho}(N_x)$ for both proteins are independent of concentration; thus, significant measured $R_{ex,\rho}(N_x)$ values are not the result of aggregation.

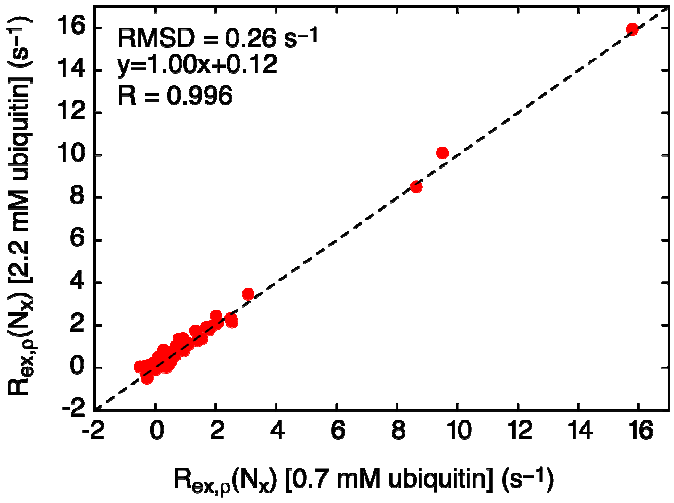

Figure S4. $R_{ex,\rho}(N_x)$ rates measured for human ubiquitin derived at two different protein concentrations, 2.2 mM and 0.7 mM (18.79 T and 278 K). The dotted line is $y=x$, R is the Pearson coefficient of linear correlation, and RMSD= $\sqrt{\sum (R_{ex,\rho}^{0.7mM}(i) - R_{ex,\rho}^{2.2mM}(i))^2 / N}$.

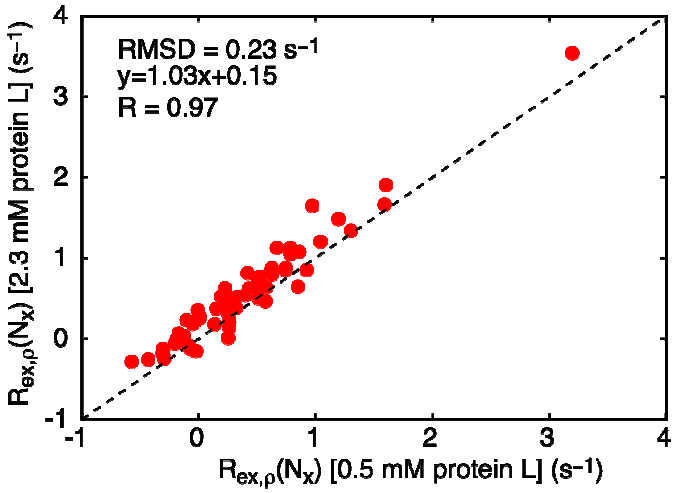

Figure S5. $R_{ex,\rho}(N_x)$ rates measured for protein L derived at two different protein concentrations, 2.3 mM and 0.5 mM (18.79 T and 278 K). The dotted line is $y=x$, R is the Pearson coefficient of linear correlation, and RMSD= $\sqrt{\sum (R_{ex,\rho}^{0.5mM}(i) - R_{ex,\rho}^{2.3mM}(i))^2 / N}$.

The effect of remote proton spins on $R_{ex,\rho}$ rates calculated from Eq. [7].

In order to estimate the contribution from external proton spins to ϑ_N (Eq. [7]) computations have been done using the X-ray structure of protein L (pdb: 1HZ6[4]) assuming either U-[^{1}H,^{15}N] isotope labeled protein or U-[^{2}H^{ali},^{15}N,^{1}H^N] isotope labeled protein (used in this study). The percentage contribution to the relaxation from the remote spins (compared with the dipolar relaxation due to the intra-residue ^{1}H^N) was calculated as $(r_{eff}/1.02\text{Å})^{-6}$, where $r_{eff}^{-6} = \sum r_{N,H_i}^{-6}$ and $r_{N,Hi}$ is the distance between the nitrogen atom in question and the external protons spins. The sum includes all protons in the protein for the U-[^{1}H,^{15}N] isotope labeled sample, while only amide protons were included for the computation involving the U-[^{2}H^{ali},^{15}N,^{1}H^N] isotope labeled protein. Figure S6 shows the percentage contribution to the dipolar relaxation of the nitrogens from external spins of

protein L. Very small contributions are calculated for the deuterated sample (approximately 0.2% for beta sheet and 0.7% for alpha helix), where 1% corresponds to ~0.1s^{-1} for protein L at 278K, much less than the accuracy of measured $R_{ex,\rho}(N_x)$ values.

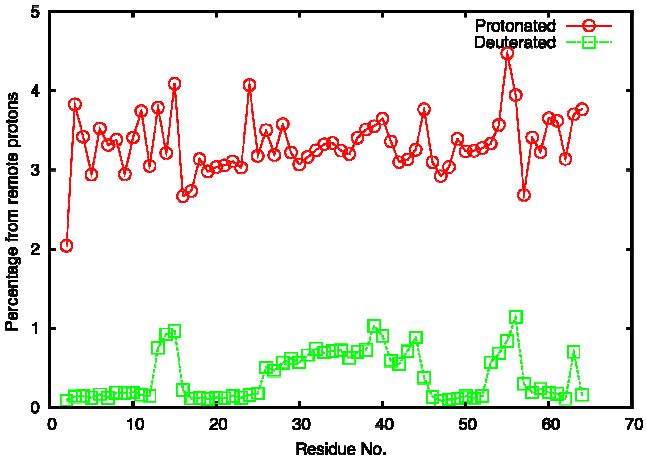

Figure S6. The contribution to the derived $R_{ex,\rho}(N_x)$ rates from external proton spins (ϑ_N of Eq. [7]) simulated for either U-[^{1}H,^{15}N] (protonated, red) or U-[^{2}H^{ali},^{15}N,^{1}H^{N}] (deuterated, green) protein L. The secondary structure elements are: β-sheet: residues 4-11, 15-23, 47-51, 56-62 α-helix: residues 26-43.

References

(1) Lundström, P.; Akke, M. *J Biomol NMR* **2005**, *32*, 163-73.

(2) Allard, P.; Helgstrand, M.; Hard, T. *J. Magn. Reson.* **1998**, *134*, 7-16.

(3) Korzhnev, D. M.; Neudecker, P.; Mittermaier, A.; Orekhov, V. Y.; Kay, L. E. *J Am Chem Soc* **2005**, *127*, 15602-11.

(4) O'Neill, J. W.; Kim, D. E.; Baker, D.; Zhang, K. Y. J. *Acta Crystallogr., Sect D: Biol. Crystallogr.* **2001**, *57*, 480-487.